Advanced International Journal for Research (AIJFR)
E-ISSN: 3048-7641 ● Website: www.aijfr.com ● Email: editor@aijfr.com

Stability of Hypersonic Boundary Layers on Circular Cones: Effect of Nose Bluntness

Suman S Goudar[1], Jayahar Sivasubramanian[2]

[1,2] Department of Aerospace and Automotive Engineering, M. S. Ramaiah University of Applied Sciences, Bangalore

Abstract

The nose bluntness is one of the key design parameters as it determines the aerodynamic characteristics of the body. Studies have shown that it also affects the stability of the body and plays an important role in determining the transition location. In this work, cones with varying nose radius are compared for the aerodynamics and the stability characteristics. A sharp cone is analyzed as the base geometry to understand the effect of nose bluntness. The domain is discretized using fine structured grids with high density near the surface to better capture the boundary layer features. First, laminar simulations of the flow over the cones were carried out using the Stanford University Unstructured (SU2) CFD solver. The boundary layer profiles were then extracted and validated with the profiles from literature. Subsequently, these profiles were fed into a python code to obtain the input file with the derivatives needed for the LST solver. The Eigen value spectrum obtained from the LST solver is analyzed for various frequencies and presence of the unstable Mack instability mode is captured if present. The procedure is repeated for various streamwise locations to obtain the Neutral Stability diagrams for different cones with varying nose bluntness. The laminar flow-field is also analyzed to understand the change in flow features with increase in bluntness. It was observed that the instability region moves downstream with increase in nose radius. Hence increase in nose radius has a stabilizing effect on the flow.

Keywords: Nose Bluntness, Stability, Hypersonic Boundary Layer, Transition, Linear stability theory (LST).

1. Introduction

Linear Stability Theory is mainly based on the individual sine waves propagating in the boundary layer parallel to the surface [1]. We know that laminar flow is acted on by various disturbances which can arise from the freestream, wall roughness, acoustic noise etc. The nature of the flow depends on the growth or diffusion of disturbances in time. If the disturbances die away or diffuse out, the laminar flow is said to be stable, and if there is a growth or amplification of disturbance in time, the laminar flow is unstable and therefore transition to turbulence takes place. Such waves which amplify and cause instability in the BL are often referred to as Tollmein-Schlichtling waves or simply T-S waves in the case of low-speed (incompressible) boundary layers. This work, however, focuses on this type of instability waves in the BL but for hypersonic Mach numbers.

The results of LST are often presented in the form of neutral stability diagram. The neutral stability diagrams are graphs of Reynolds number vs ω or Reynolds number vs α or Reynolds number vs frequency.

Wherever the values of phase velocity are equal to zero, this curve separates the stable region from unstable region. The smallest Reynolds number on this curve for which instable region exists is known as the Critical Reynolds number. The disturbances are damped for Reynolds number less than the critical Reynolds number and are amplified for those greater than the critical Reynolds number. A typical, neutral stability curve is presented in Figure 1 [6].

The analysis of stability of hypersonic boundary layers is challenging owing to many factors. Hypersonic BL is characterized with many types of instability, namely Mack first mode instability, Mack second mode instability, Gortler instability arising due to curvature effects, and Crossflow instability arising due to 3D effects [2]. The Gortler and Crossflow instability analysis is out of scope of this research work. The second mode instability is the most amplified in hypersonic BLs and it is recognized to be the dominant mode which induces transition in hypersonic BL [5, 6]. The current work's focus revolves around capturing the dominant second mode as the first mode is least amplified or absent in two-dimensional/axis-symmetric boundary layers.

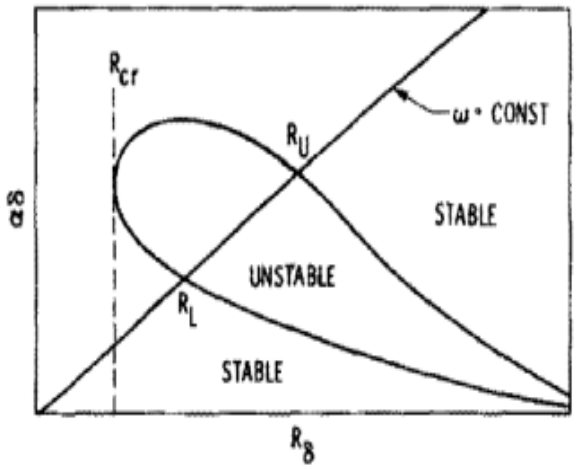

Figure 1: Neutral Stability Curve [6]

2. Literature Review and Objective

The flow conditions are obtained from the approach flow conditions in the cone experiments conducted in the Boeing Mach 6 quiet flow tunnel at Purdue University [9]. The temperature of the wall is higher than the temperature of the free-stream flow i.e. it is a hot wall. The approach flow is cold to minimize the disturbances and laminarize the wall bounded flow in the nozzle of the wind tunnel. The free stream conditions considered are mentioned in Table 1.

Table 1: Freestream conditions considered for Base flow (mean flow) simulations.

Unit Reynolds Number (m-1)	10.5×10^6
Mach Number	6
Total Temperature (K)	430
Total Pressure (kPa)	1043

Free Stream Temperature (K)	52.4385
Free Stream Pressure (kPa)	660
Wall Temperature (K)	300

The cone model used in Purdue experiments has a half angle of 7^{o}. The length of the cone is 0.517m [10]. The radius of the sphere nose is $5e^{-5}$m which is a very small and therefore the cone can be considered as a sharp cone. In addition, two blunt cone cases are considered. The half angle of the cone remains the same but the length of the cone is increased to 3m to capture the downstream moving instability region and the transition location. The radius of the sphere blunted nose is 2.54mm and 7.62mm for the two cases considered in this study. The main objective is to analyse the stability characteristics of hypersonic flow and gain insights into the stability and transition physics.

3. Methods and Methodology

The discretization of the entire two-dimensional/axis-symmetric flow domain was performed using Pointwise grid generation software. A structured grid with grid density concentrated close to the wall region was utilized to obtain accurate boundary layer profiles as shown in Figure 2a, b and c. The grid is maintained perpendicular/normal to the cone wall to facilitate the extraction of the boundary layer profiles. The domains for the blunt cone cases were increased to capture the downstream moving instability region as seen in Figure 2b. No-slip boundary condition is applied to the cone wall. Pressure far field boundary condition was applied to the boundary parallel to the wall and the nose surface. Pressure outlet Boundary condition is applied for the boundary perpendicular to cone wall with the values mentioned in table 1.

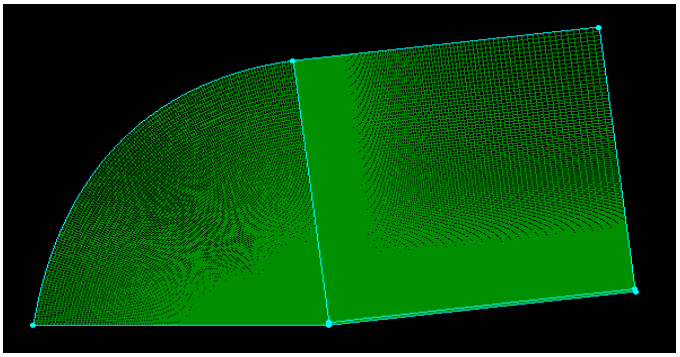

Figure 2a: Computational domain for sharp cone

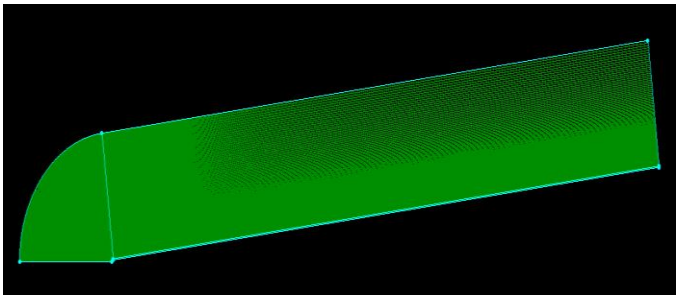

Figure 2b: Elongated domain for blunt cone

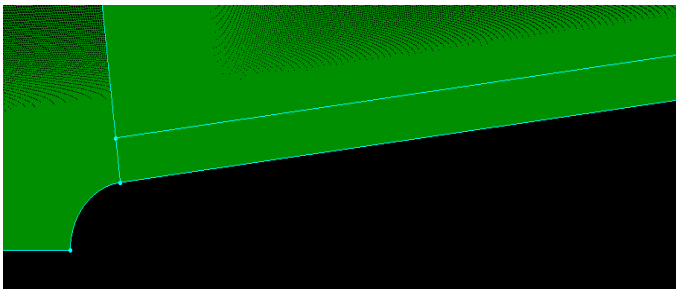

Figure 2c: High resolution grid distribution near the wall to capture the boundary layer

The laminar base flow (mean flow) axisymmetric simulations are carried out using the Stanford University Unstructured CFD solver, popularly known as SU2. The fluid is considered to be an ideal gas irrespective of the high Mach number of the free stream flow as the enthalpy of free stream is very low. The solver setup is summarized in table 2.

Table 2: CFD Solver Setup.

Solver Type	Navier-Stokes Density based solver
Fluid Model	Ideal Gas
Viscosity Model	Sutherland's Viscosity Model
Convective Flow Numerical Method	AUSMPLUSUP

The velocity, temperature and viscosity profiles are extracted perpendicular to wall using the commercial software Tecplot. These values are then normalized with respect to the boundary layer edge values. For blunt cases, though there is variation in the boundary layer edge values with variation in x near the nose region, it remains almost a constant away from the nose.

4. Results and Discussion

A. Aerodynamic Analysis

The velocity profiles obtained from the laminar base flow (mean flow) simulations are in good accordance with the literature [10] as shown in Figure 3a. The thickness of the boundary layer increased downstream and also with increase in nose radius (see Figure 3b).

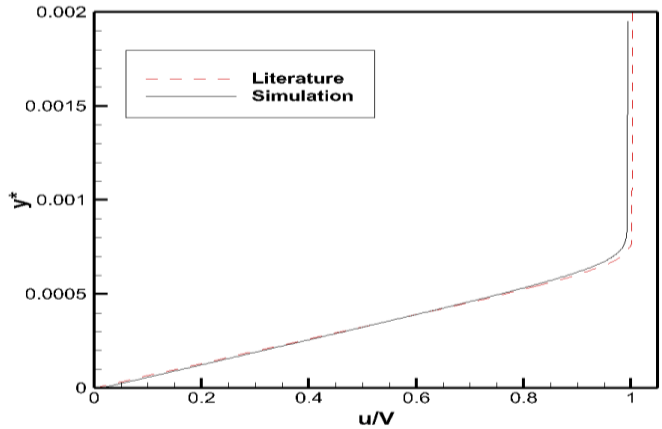

Figure 3a: Validation of results obtained for sharp cone at x=0.1m

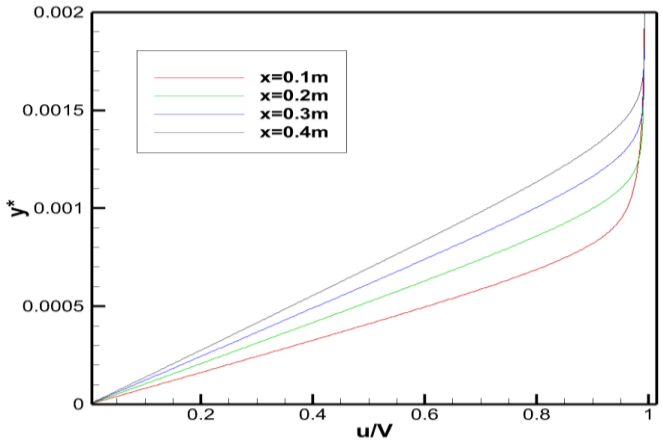

Figure 3b: Comparison of velocity profiles for the sharp cone at different streamwise locations.

The freestream high energy kinetic flow is slowed down by viscous effects and a shock is formed at the nose of the cone. The type of shock depends on the shape of the nose as seen in Figures 4a and b. A clear distinction is observed in the Mach number contours of the sharp and blunt cones. Different kind of shock waves formed is the reason for this distinction. A weak oblique shock is observed on the sharp cone whereas a strong bow shock is observed on the blunt cone. The bow shock is normal to the flow direction near the nose and hence a small subsonic region is observed between the shock and nose. Initially, the oblique part of the bow shock turns the flow towards itself. But for the flow to be parallel to surface, it must be turned away from the oblique shock and this is accomplished by the formation of series of expansion waves. These expansion waves are absent in sharp cone as oblique shock turns the flow parallel to the surface eliminating their need. We can also witness the small region of boundary layer in both the contours.

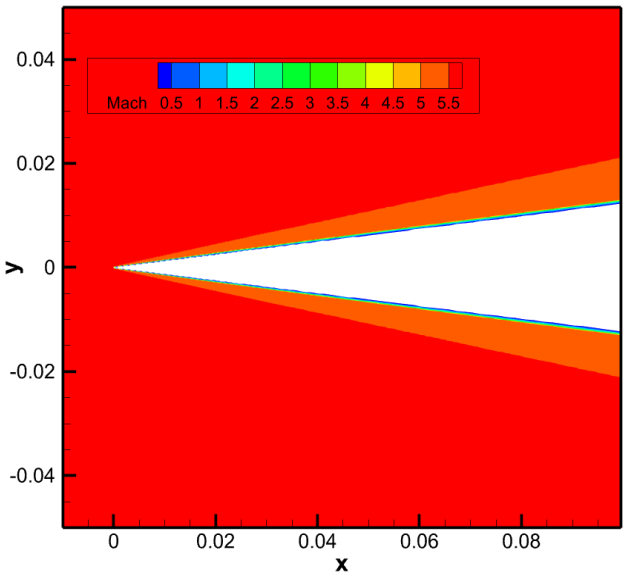

Figure 4a: Contours of Mach number for sharp cone.

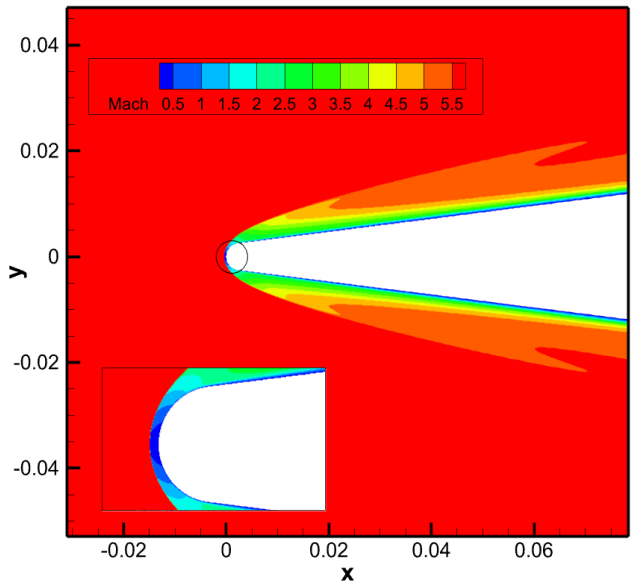

Figure 4b: Contours of Mach number for blunt cone with nose radium 2.54mm.

The temperature contours are also distinct for both cases as expected. They are represented in Figure 5a and b. The growth of thermal BL is observed in the blunt nose case. In the sharp cone, the stagnation point experiences the highest temperature where in blunt cone the region between the nose and the normal portion of the bow shock experiences high temperature. This leads to less heat transfer in blunt cones compared with sharp cones.

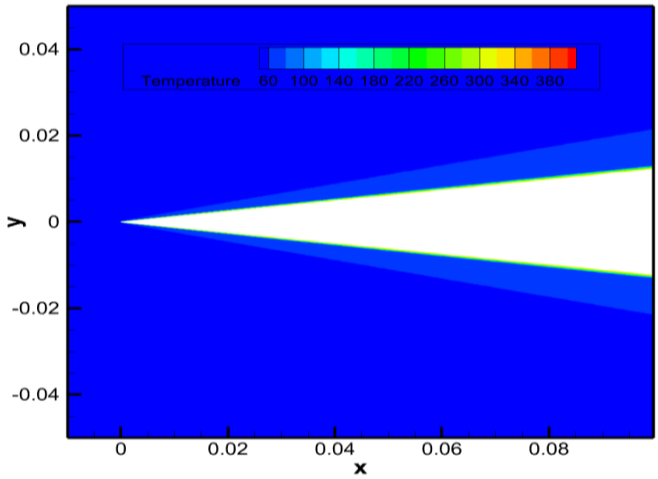

Figure 5a: Contours of temperature for sharp cone.

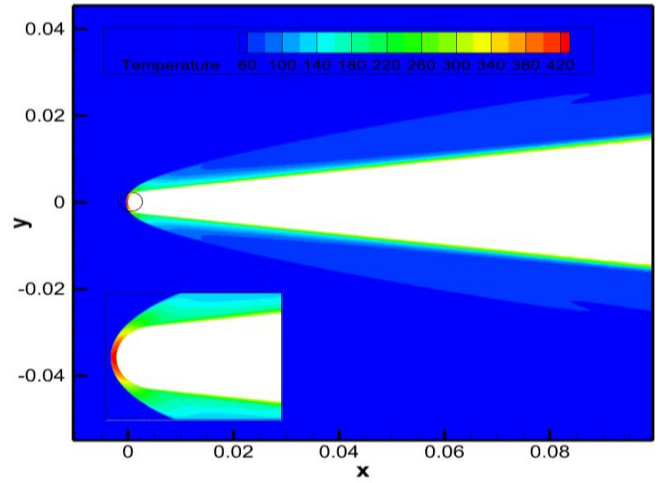

Figure 5b: Contours of temperature for blunt cone with nose radius 2.54mm.

The local Reynold's number decreases with the increase in nose radius as the velocity of the freestream decreases owing to a stronger bow shock formed. This is one of the main reason why the unstable region and hence the transition location itself moves downstream with increase in nose radius. The skin friction coefficient in the stagnation region is higher due to high wall shear stress for the sharp cone as shown in Figure 6. The sharp cone experiences highest C_f as it is exposed to hypersonic Mach 6 flow whereas the blunt cones are exposed to only subsonic flow after the incoming free stream passes through a strong bow shock. Therefore, the shear stress acting on sharp noses is more than that of blunt noses. We can also observe that the point of maximum C_f moves downstream as we increase the nose radius. Further downstream no variation is observed between the sharp and blunt cones as the flow conditions are similar for all the cases away from the nose.

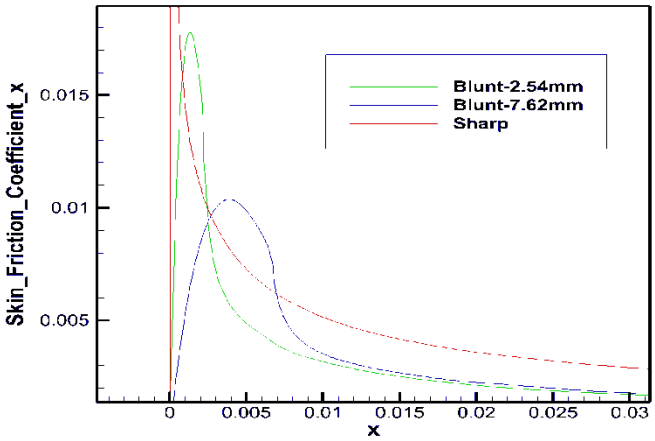

Figure 6: Comparison of skin friction coefficient for different cones.

The heat flux observed is maximum in the stagnation region as the kinetic energy of the flow is converted into the internal energy of the fluid. The decrease in heat flux is gradual with the increase in nose radius which can be attributed to the local variation in surface temperature near the nose. There is a decrease in maximum heat flux at the stagnation region as the nose radius increases due to the dissipation in the region between the bow shock and the nose. The reduction in heat transfer is nearly 75% for 2.54mm nose radius and 86% for 7.62 nose radius. This proves the effectiveness of blunt cone in reducing the heat load on the vehicle and on the requirement of TPS. The trends observed for skin friction and heat flux is the same for all the cases. We can observe that the skin friction coefficient and heat flux follow the same trend.

Table 3: Variation of maximum Heat Flux for different cones.

Nose radius (m)	***Heat Flux (W/m^2)***	***Percentage decrease (%) (with respect to sharp cone)***
5e-05 - Sharp	547283	-
0.00254 - Blunt	133509	75.601
0.00762 - Blunt	76036	86.106

B. Stability Analysis

The velocity profiles extracted are fed into the python code and the input files for LST are obtained. The output of LST solver is the Eigen value spectrum of the complex streamwise wavenumber. The spectrum is presented in Figure 8. The spectrum represents the values of the streamwise wavenumber of all the possible disturbances or perturbations in the boundary layer. The spectrum is comprised of continuous and discrete spectra. The discrete spectra are the cause of instability in the BL. It is also not necessary that all discrete spectra will cause instability in BL. If the complex component of wavenumber of the discrete spectra is negative, such waves are called amplified waves which induce instability in the BL. The spectrum has three continuous branches. The horizontal branches represent the acoustic modes and the vertical branch represents the entropy and vorticity modes. The vorticity and the entropy modes are

indistinguishable in Figure 7 but they do not overlap each other. Sometimes the discrete modes of acoustics are observed as in Figure 7a and these modes are called fast and slow acoustic modes. The interaction between these modes is also a factor which determines the transition location.

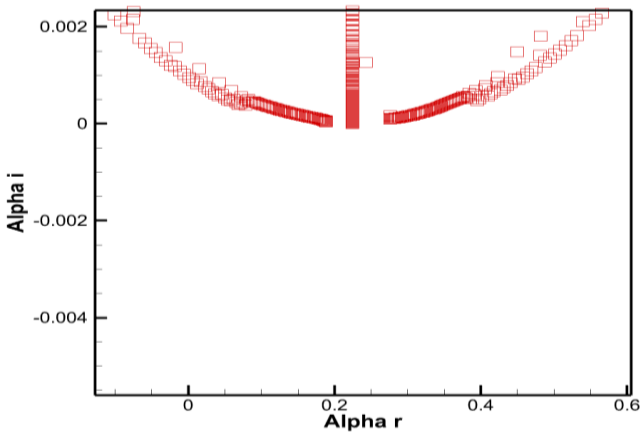

Figure 7a: Eigenvalue spectra with no unstable discrete mode for sharp cone at x=0.12m and f=320kHz.

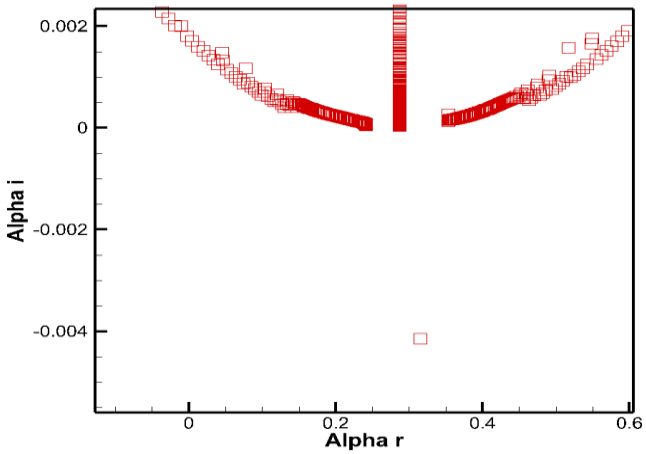

Figure 7b: Eigenvalue spectra with unstable discrete mode for sharp cone at x=0.12m and f=408kHz.

The LST solver was run for various locations at different frequency to obtain the Neutral Stability curve for second mode or Mack mode instability (see Figure 9). We can observe that the instability creeps in the flow at location x=0.015m from the nose. The critical Reynolds number at x=0.015 is 418. The region inside the curve represents the instability region and the region outside the curve is the stable region. The points on the curve represent neutral waves, i.e. the amplitude remains constant. It was observed that the amplification factor increased as we move downstream reaching a peak value and then it decreases as shown in Figure. 8. There are high chances of non-linearity taking over the BL at the peak amplification point and the flow may transition to turbulence. It is also important to note that the critical Reynold's number obtained from linear stability theory does not exactly predict the transition location but rather the onset of instability. These instabilities further grow downstream and finally breakdown to turbulence. The neutral stability curves for blunt cones are also obtained in the same way as the sharp one. As the nose

radius increases, the transition location moves downstream [9]. We can observe that the neutral stability diagram has shifted downstream and has spread into the lower frequency ranges as observed in [5]. We can say that as the thickness of the boundary layer increases the perturbation frequency decreases. We can also observe that the frequency band of the instability region increases with increase in nose radius. This might be bit misleading because even though the instability region frequency band increases, their amplification factor reduces considerably as shown in Figure 10.

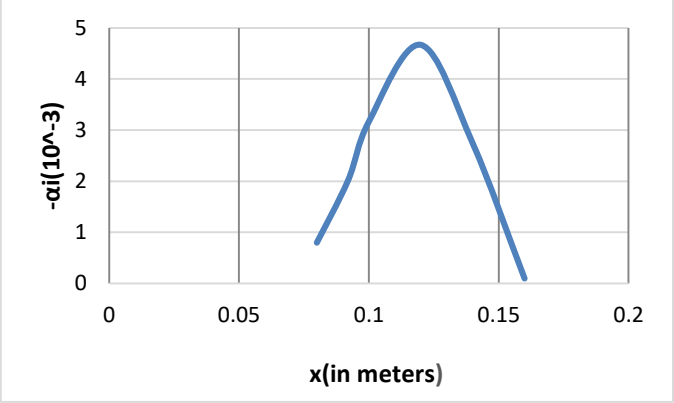

Figure 8: Variation of amplification factor for sharp cone at 400kHz

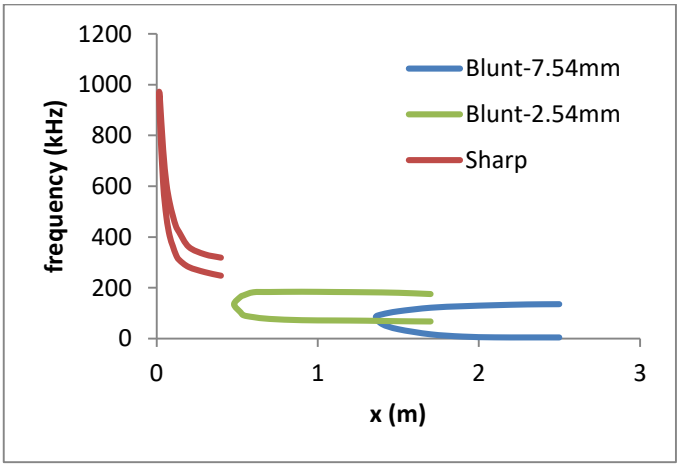

Figure 9: Comparison of Neutral Stability curve for different Cones.

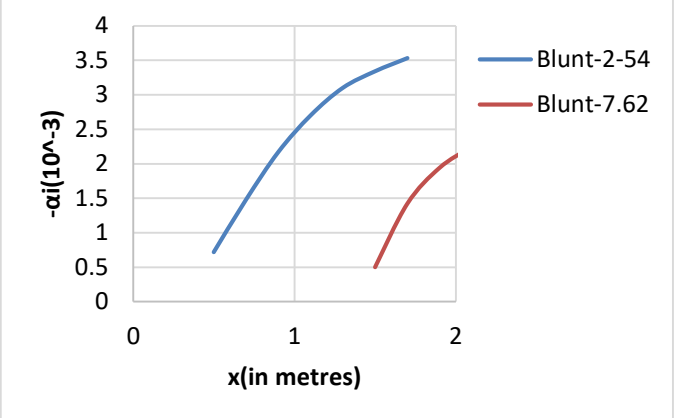

Figure 10: Comparison of amplification factor of Blunt Cones at frequency 100kHz

Table 4: Comparison of critical Re number for different cones.

Nose Radius (m)	Instability onset location (m)	Critical Reynolds Number
5e-05 - Sharp	0.016	418
0.00254 - Blunt	0.48	2367
0.00762 - Blunt	1.37	3997

5. Conclusions

The instability onset location and hence the transition location itself moves downstream with increase in nose radius (bluntness) indicating its stabilizing effect. The difference in the mean flow and the profiles is the main reason for the observable changes in stability characteristics. 2D Axisymmetric simulations proved to a right choice to capture the dominant 2D second mode instabilities. Stability results obtained here are in good accordance with the literature. The assumption of absence of the Mack first mode in two-dimensional/axis-symmetric boundary layers is also validated as there were no unstable modes found in the lower frequency band. Stability characteristics are highly sensitive to the base flow boundary layer profiles. SU2 proved to be a right choice of software as it produced BL profiles with high accuracy to match the literature. Blunt cones with small nose radius were found to be favourable for hypersonic vehicles based on both the aerodynamic and stability analysis.

References

1. Alexander V, Fedorov, (2015), "*Prediction and Control of Laminar-turbulent Transition in High-speed Boundary-Layer Flows*", *Procedia IUTAM*, Volume 14, 2015.
2. Anderson, J., (2011). *Fundamentals of Aerodynamics* (SI units). McGraw Hill.
3. Fransson, J., & Shahinfar, S. (2020), "*On the effect of free-stream turbulence on boundary-layer transition*", *Journal of Fluid Mechanics*, 899, A23.
4. H. Schlichting, (1979) *Boundary Layer Theory*, 7th edition, McGraw-Hill, New York, 1979.

5. Lei, J. and Zhong, X., (2012). "*Linear stability analysis of nose bluntness effects on hypersonic boundary layer transition*". *Journal of Spacecraft and Rockets*, 49(1), pp. 24-37.
6. Mack, L.M., (1984). "*Boundary-layer linear stability theory*". California Inst. of Tech. Pasadena Jet Propulsion Lab.
7. Narayan, A., Narayanan, S. and Kumar, R., (2018). "*Hypersonic flow past nose cones of different geometries: a comparative study*". *Simulation*, 94(8), pp.665-680.
8. Porter, L.M., Mee, D.J., Simmons, J.M., Davis, M. and Walker, G., (1992). "*Measuring the Effect on Drag Produced by Nose Bluntness on a Cone in Hypervelocity Flow*". In Proc. 11th Australasian Fluid Mechanics Conference (Eds DAVIS, M. and WALKER, G.), University of Tasmania, Hobart, Australia (pp. 287-290).
9. Schneider, S.P., (2004). "*Hypersonic laminar–turbulent transition on circular cones and scramjet forebodies*". *Progress in Aerospace Sciences*, 40, pp. 1-50.
10. Sivasubramanian, J. and Fasel, H.F., (2015). "*Direct numerical simulation of transition in a sharp cone boundary layer at Mach 6: fundamental breakdown*". *Journal of Fluid Mechanics*, 768, pp.175-218.
11. Tumin, A., (2007). "*Three-dimensional spatial normal modes in compressible boundary layers*". *Journal of Fluid Mechanics*, 586, pp. 295-322.